Journal of Materials Chemistry A

PAPER

A ZnO nanorod/nanoparticle hierarchical structure synthesized through a facile *in situ* method for dye-sensitized solar cells†

Cite this: *J. Mater. Chem. A*, 2014, **2**, 4765

Rui Gao,[a] Yixiu Cui,[a] Xiaojiang Liu,[a] Liduo Wang*[b] and Guozhong Cao*[cd]

Received 18th December 2013
Accepted 13th January 2014

DOI: 10.1039/c3ta15276f

www.rsc.org/MaterialsA

A novel ZnO nanorod/nanoparticle (NR/NP) hierarchical structure on a zinc foil has been fabricated through a chemical bath deposition method. When used as a flexible photoanode for DSSCs, such a structure demonstrated enhanced dye-loading and electron lifetime as compared to the NR structure. It also retarded the charge recombination while maintaining the electron diffusion length of the NR structure. As a result, the power conversion efficiency of the DSSCs based on the NR/NP structure increased from 1.35% to 3.63% with a 169% enhancement as compared to that based on ZnO NRs.

1. Introduction

Since the breakthrough in power conversion efficiency reported in 1991,[1] dye-sensitized solar cells (DSSCs) have been considered as an alternative to the conventional silicon based solar cells due to their lower cost and easier fabrication as well as low sensitivity to the incident angle and the intensity of light. By 2011, a high power conversion efficiency of 12.3% was achieved,[2] which is close to the efficiency of commercial silicon solar cells. Much attention has been focused on efficiency enhancement and stability improvement of DSSCs.[3] Besides TiO_2, ZnO has been widely and intensively studied as a photoanode for DSSCs in recent years[4] due to its easier synthesis and higher electron mobility.[5] A high conversion efficiency of 7.5% was achieved in 2011.[6] Furthermore, ZnO DSSCs based on quasi-solid electrolytes also exhibited high conversion efficiency,[7–9] which is up to 6.46%.[10]

Flexible DSSCs have attracted significant interest because of their lightweight, low cost roll-to-roll production and potential applications in powering mobile electronic products. Until now, two kinds of flexible substrates have been used, metal sheets[11] and polymer substrates.[12] Compared to polymer substrates, metal sheets have lower resistance, and are easier for making flexible DSSC devices.[11,13] However, DSSC devices based on metal sheets exhibit much lower conversion efficiency than that based on FTO glass.[14,15] As a result, much study has been done to enhance the efficiency of such types of DSSCs.[16,17]

Due to its high electron mobility, ZnO with ordered structures, especially one-dimensional nanostructures, was considered as an ideal structure for photoanodes.[18–21] ZnO nanotubes and nanorods have been synthesized and they are used to fabricate DSSCs with high conversion efficiency. However, the 1-D structures have a much smaller surface area for dye adsorption when compared with nanoparticles, resulting in a lower photocurrent and efficiency. Constructing hierarchical morphologies based on 1-D structures and nanoparticles turns out to be an effective way to improve the surface area significantly.[22] Cao *et al.* developed nanoparticles and nanorod array hybrid photoanodes and achieved a 4.24% conversion efficiency.[23] Recently, a ZnO nanorod–nanoparticle hierarchical structure has been used in DSSCs, which showed a high conversion efficiency of 7.14%.[24] However, the synthesis method used needs high temperature,[25] which increases the power consumption and cost.[26] The direct precipitation process[27,28] is an efficient way to synthesize ZnO with specific shapes at low temperature.[29,30] Herein, we report an *in situ* precipitation method[31] to synthesize nanoflowers composed of nanorods (NR) on the zinc foil which could be used as flexible photoanodes for DSSCs.[32] Compared with other routes such as electrochemical deposition, physical/chemical vapor deposition or hydrothermal methods, this method features simpler operation and lower cost, and is more ideal for industrial production. To improve the performance of DSSCs based on such photoanodes, a nanorod/nanoparticle (NR/NP) hierarchical structure has been fabricated by a chemical bath deposition (CBD) method in a $Zn(OAc)_2 \cdot 2H_2O$ methanolic solution. The ZnO NR/NP composite photoanode fabricated combines the high electron transport abilities and large dye absorption areas, thereby significantly increasing the conversion efficiency of DSSCs based on flexible photoanodes.

[a]*Institute of Electronic Engineering, China Academy of Engineering Physics, Mianyang 621900, Sichuan, China*

[b]*Key Lab of Organic Optoelectronics & Molecular Engineering of Ministry of Education, Department of Chemistry, Tsinghua University, Beijing 100084, China. E-mail: chldwang@mail.tsinghua.edu.cn*

[c]*Department of Materials Science and Engineering, University of Washington, Seattle, WA 98195, USA. E-mail: gzcao@u.washington.edu*

[d]*Beijing Institute of Nanoenergy and Nanosystems, Chinese Academy of Sciences, Beijing 100085, China*

† Electronic supplementary information (ESI) available. See DOI: 10.1039/c3ta15276f

2. Experimental

An alkaline zincate solution was prepared by dropping 20 mL 0.125 M aqueous solution of $Zn(NO_3)_2 \cdot 6H_2O$ into 20 mL 1.0 M aqueous solution of KOH under stirring. The growth of ZnO nanorod assembled nanoflowers was achieved by suspending a clean zinc foil (Alfa Aesar, 99.9%, 0.25 mm thick) upside down in 40 mL zincate solution and sealing the system in a beaker. The zinc foil was feathered by sanding and then cleaned through ultrasonic vibration in pure ethanol before use. After reaction at 40 °C for 4 h, the zinc foil was taken out and rinsed with de-ionized water. The second process consisted of transferring the zinc foil obtained in the last process into a 20 mL glass bottle containing 0.01 M $Zn(OAc)_2 \cdot 2H_2O$ methanolic solution, and heating at 40 °C for 12 h.

The ZnO photoanode was sintered at 350 °C, then sensitized in 0.3 mM N719 absolute ethanol solution for 60 min, followed by cleaning with absolute ethanol. The electrolyte is a liquid admixture containing 0.5 M tetrabutylammonium iodide, 0.1 M lithium iodide, 0.1 M iodine, and 0.5 M 4-*tert*-butylpyridine in acetonitrile. A transparent platinized conductive glass was used as the counter electrode, which was bought from Dyesol Ltd. directly. When assembling the back-illuminated DSSCs, the electrolyte was sandwiched between a sensitized ZnO on the zinc foil and a counter electrode with two clips. A 60 μm thick adhesive tape was used to separate the photoanode and the counter electrode. The illumination was from the direction of the counter electrode.

The UV-Vis reflectance absorption spectra were measured using a Hitachi U-3010 spectroscope. The morphologies of the ZnO films were characterized by SEM (JSM 7401). Photocurrent–voltage (*I–V*), dark current measurements, monochromatic incident photon-to-electron conversion efficiency (IPCE), electrochemical impedance spectroscopy (EIS) and the intensity modulated photovoltage/photocurrent spectrum (IMVS/IMPS) were investigated using a ZAHNER CIMPS electrochemical workstation.

3. Results and discussion

Different ZnO structures have been fabricated on a zinc foil through a precipitation method at different temperatures. Fig. 1(a) and (b) show that as the reaction proceeds at a lower temperature (20 °C), the precipitation is difficult to occur, forming a disordered nanoparticle structure. As the reaction temperature was increased to 40 °C, nanorod assembled nanoflowers (NFs) were obtained on the zinc foil, which are shown in Fig. 1(c) and (d). The size of the NFs is about 1–1.5 μm. As the reaction temperature was further increased to 60 °C, part of ZnO nanorods turned into nanosheets. At the same time, the size of the NFs also increased to about 3 μm, as seen in Fig. 1(e) and (f). The formation process of hierarchical structures is shown in Fig. 1(c) and (e) which is similar to that reported in ref. 7.

We tested the photovoltaic performance of DSSCs based on different ZnO structures obtained at different reaction temperatures which are shown in Fig. 1. As shown in Fig. 2, the device based on ZnO NR assembled nanoflowers synthesized at 40 °C showed the highest V_{oc}, J_{sc} and conversion efficiency, which was 1.35% under 100 mW cm^{-2} illumination. It could be explained that the NR assembled nanoflowers combined efficient dye-loading and good electron transport. When the reaction temperature is as low as 20 °C, disordered ZnO nanoparticles are formed. The nanoparticles could not adsorb dye molecules efficiently, thus the photocurrent is rather low. As the reaction temperature is increased to 60 °C, the dye-loading capacity of the ZnO photoanode could become lower than that obtained at 40 °C as the nanosheet assembled nanoflowers are much larger than the NR assembled sample, which could cause a decrease in the specific surface area. The verified V_{oc} and FF with different morphologies of ZnO could be explained as follows. At a

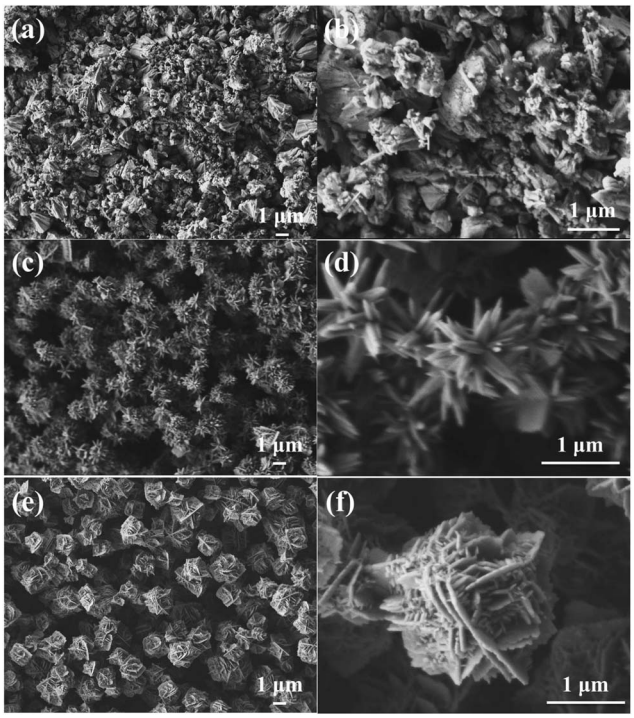

Fig. 1 SEM images of different ZnO films on the zinc foil obtained by the precipitation method at different temperatures (a and b) 20 °C, (c and d) 40 °C and (e and f) 60 °C.

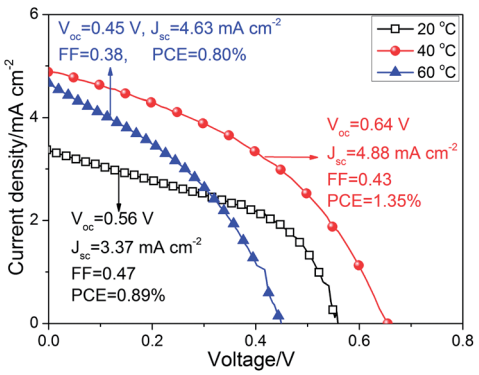

Fig. 2 *I–V* curves under 100 mW cm^{-2} illumination of DSSCs based on ZnO obtained by the precipitation method at different temperatures.

reaction temperature of 20 °C, we obtained a disordered structure, which has poor electron transport in the ZnO film. Thus the charge recombination increased. Compared to the sample obtained at 60 °C, the 40 °C sample has a smaller sized nanoflower structure, which could cause a better connection between different nanoflowers. Furthermore, the 40 °C sample with a 1-D structure exhibits better electron transport than the 2-D structure of the 60 °C sample. As a result, the possibility of charge recombination is smaller than that for the 60 °C sample. As a result, the V_{oc}, J_{sc} and FF of the 60 °C sample all decreased compared to the 40 °C sample.

The growth of ZnO on a zinc foil could be represented by the following reactions[31]

$$Zn + 2H_2O + 2OH^- \rightarrow Zn(OH)_4^{2-} + H_2 \quad (1)$$

$$Zn(OH)_4^{2-} \rightarrow ZnO + H_2O + 2OH^- \quad (2)$$

At first, the dissolution of Zn atoms into the solution caused a concentration gradient of zincate ions, and then NR arrays are formed on the zinc foil (see Fig. S1†) during the precipitation reaction in a short time at 40 °C, which is the same as that reported in ref. 28. When the precipitation process continued, more and more ZnO particles deposited onto the zinc foil. The NR arrays could strengthen the connection of the zinc foil and ZnO precipitated on it, which could benefit electron transfer from ZnO to the zinc foil.

As shown in Fig. 3, the HRTEM image revealed that the NRs are a single crystal. According to the features of the diffraction pattern, the preferential growth direction of the ZnO NRs is [001]. The displayed lattice spacing of 0.26 nm corresponds to the lattice spacing of the ZnO (002) plane, which also indicates that the [001] direction is the preferential growth direction.[33] During the process of ZnO nanocrystal growth, the dissolution of Zn atoms into the solution caused a concentration gradient of zincate ions from the bottom to the top of NRs. As a result, the growing rates along the ZnO (001) planes decreased from the nanocrystal roots to the tips and finally NRs shown in Fig. 1(c) and (d) and Fig. 3 were formed. This could be explained by the fact that the excess OH^- anions retarded the growth of other facets. This result also is in accordance with that in ref. 31. However, the effect of the concentration gradient was weakened by increasing the reaction temperature as it could cause a much faster growth of ZnO nanocrystals. Thus as the reaction temperature increased to 60 °C, besides the [001] direction, ZnO growth in the [100] direction started to appear, forming the nanoflowers composed of nanosheets as shown in Fig. 1(e) and (f).

As shown in Fig. 2, the 40 °C sample exhibited the highest efficiency of 1.35% of the three different samples. However, one key challenge in using such a 1D nanostructure in DSSCs is their relatively lower specific surface area compared to nanoparticles, resulting in insufficient dye adsorption and, therefore, low light-harvesting efficiency. Hierarchical morphologies consisting of 1-D nanorods and 0-D nanoparticles would offer an effective way to synergistically combine the high specific surface area with easy and fast charge transfer. Thus we fabricate such a hierarchical structure of ZnO NRs/NPs through a chemical bath deposition method in $Zn(OAc)_2 \cdot 2H_2O$ methanolic solution.

As shown in Fig. 4(a) and (b), after being treated in $Zn(OAc)_2 \cdot 2H_2O$ methanolic solution, nanoparticles were formed and attached onto the NRs. The surface of NRs became much rougher, which indicated that the surface area increased. As shown in Fig. 4(c) and (d), the HRTEM images reveal nanoparticles attached on the NRs and the NPs were about 10 nm in diameter. The attachment process of NPs on the NRs and sensitization are illustrated in Scheme 1. The increased surface area enhanced the amount of dye loaded. Table 1 compares the dye-loading amount in ZnO NRs with that in NRs/NPs and shows an increase from 89 nmol cm^{-2} to 162 nmol cm^{-2}, with an 86.2% relative enhancement. A large dye adsorption amount would capture more photons, resulting in a larger IPCE and J_{sc}, and thus improving the power conversion efficiency of DSSCs.

As shown in Fig. 5(a) Table 1 shows the photovoltaic performance of DSSCs based on ZnO NR and NR/NP photoanodes. The short-circuit current density (J_{sc}) of the device based on NR is 4.88 mA cm^{-2}. As the ZnO NR/NP photoanode is applied, the J_{sc} increases to 9.40 mA cm^{-2}, enhancing 92.6% compared to ZnO NRs. As discussed above, the increased photocurrent density is due to much larger dye-loading in the NR/NP structure. Besides increasing J_{sc}, the NR/NP structure

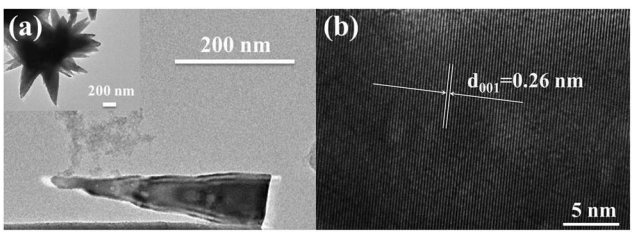

Fig. 3 HRTEM images of ZnO NR assembled nanoflowers on the zinc foil fabricated at 40 °C during the precipitation process in the alkaline solution.

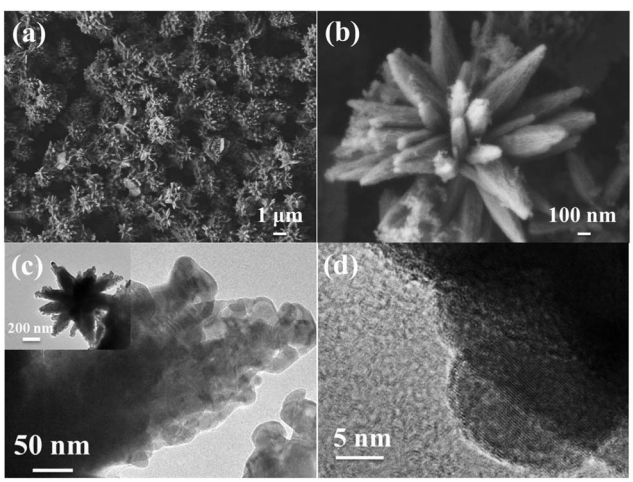

Fig. 4 (a and b) SEM images of ZnO nanoflower composed of nanorod/nanoparticles. (c and d) HRTEM images of ZnO nanorods/nanoparticles grown in 0.01 M $Zn(OAc)_2 \cdot 2H_2O$ methanolic solution heated at 40 °C for 12 h.

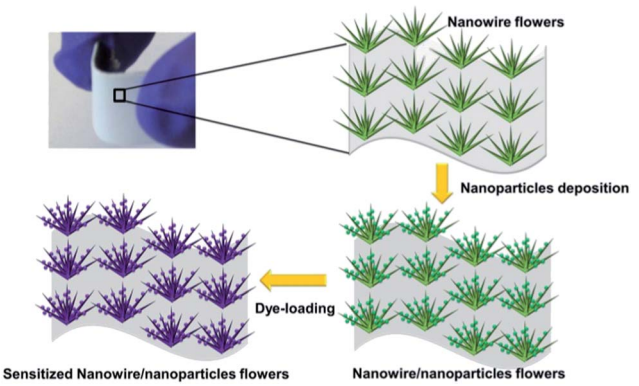

Scheme 1 Schematic illustration of nanoparticle deposition on the nanorods and sensitizing processes.

Table 1 Photovoltaic parameters of DSSCs based on ZnO NR and NR/NP photoanodes

Samples	J_{sc}/mA cm^2	V_{oc}/V	FF%	PCE/%	Dye-loading/ nmol cm^{-2}
NRs	4.88	0.64	43.2	1.35	89
NRs/NPs	9.40	0.64	60.4	3.63	162

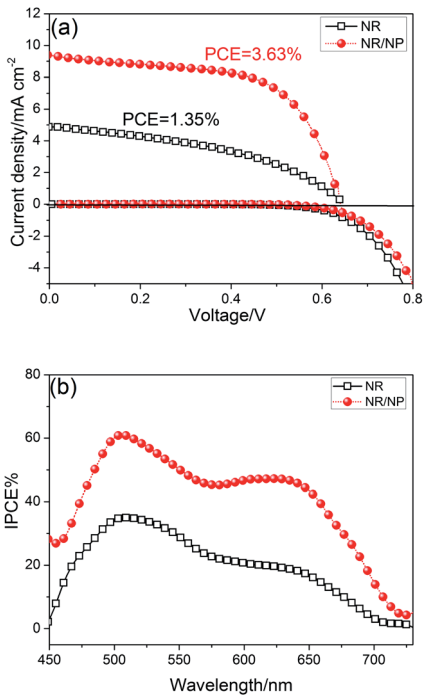

Fig. 5 (a) I–V curves (b) IPCE of DSSCs based on ZnO NRs and the NR/NP photoanode under 100 mW cm^{-2} illumination. The dark current curves are also added in (a).

also improved the FF of DSSCs compared to the device based on ZnO NRs. As shown in Fig. 5(a) and Table 1 the FF increased from 43.2% to 60.4% as the ZnO NR structure turned into the NR/NP structure. At the same time, the V_{oc} value did not change during the NP deposition process. As a result, compared to DSSCs based on ZnO NRs, the conversion efficiency of those based on the NR/NP hierarchical structure increased from 1.35% to 3.63%, showing a significant enhancement of 169%, which is high for ZnO DSSCs based on flexible metal foil photoanode. The performance stability of DSSCs based on the flexible photoanode during bending is also good. As shown in Fig. S3,† though the J_{sc} and V_{oc} decrease a little after bending, the conversion efficiency is almost maintained the same as that before bending.

As shown in Fig. 5(a), the dark current also decreased as the ZnO NR structure changed to the NR/NP hierarchical structure, indicating a weaker back reaction in devices based on such a photoanode.

As shown in Fig. 5(b), compared to the DSSC device based on the ZnO NR photoanode, the IPCE of the DSSCs based on the ZnO NR/NP photoanode increased significantly, which is about two times that of the former. The enhancement of IPCE is considered to be caused by the increased dye-loading amount as the ZnO NR structure changed to the NR/NP hierarchical structure, which is shown in Table 1. Hence, such a hierarchical ZnO photoanode would maximize the use of solar light, which enhances the light harvesting efficiency and J_{sc} of DSSCs.

To further investigate the electron transport and recombination properties of these two different structures, we tested EIS and IMVS/IMPS of DSSC devices based on ZnO NR and NR/NP photoanodes. As shown in Fig. 6(a), in the frequency range of 10^5 Hz to 10^3 Hz, the impedance associated with the charge transfer process occurring at the Pt electrode/electrolyte interface is determined, which is characterized by the charge transfer resistance (R_1) and the capacitance (CPE$_1$). In the middle frequency range of 10^3 Hz to 10^0 Hz, the impedance related to the charge recombination process at the TiO$_2$/dye/electrolyte interface can be described by R_2 and CPE$_2$. And in the low frequency range of 0.1–10 Hz, the Warburg diffusion impedance (Z_w) within the electrolyte will be estimated. The sheet resistance (R_s) of the substrate, the charge transfer resistance of the counter electrode (R_1) and the charge transfer resistance (R_2) were analyzed using Z-view software using an equivalent circuit shown in the inset of Fig. 6(a).

Z_w accounts for a finite length Warburg diffusion while CPE represents the constant phase element. As shown in Fig. 6(a) and Table 2, the cells based on ZnO NRs and NRs/NPs showed similar values of R_s and R_1. Compared to cells based on ZnO NRs, the charge recombination resistance of the cells based on ZnO NRs/NPs increased from 105 Ω to 178 Ω, indicating that charge recombination is more difficult. Thus the back reaction was decreased. The result also is in accordance with the results of dark current measurements shown in Fig. 6(b).

The weakened charge recombination could be explained by two reasons. At first, the connection could be improved during the nanoparticle deposition process, which connects several NFs together. As a result, it is easier for electrons to be collected by the zinc foil substrate, decreasing the possibility of charge recombination. Besides, during the NP deposition, the surface defect states could be passivated, thereby decreasing the charge recombination.

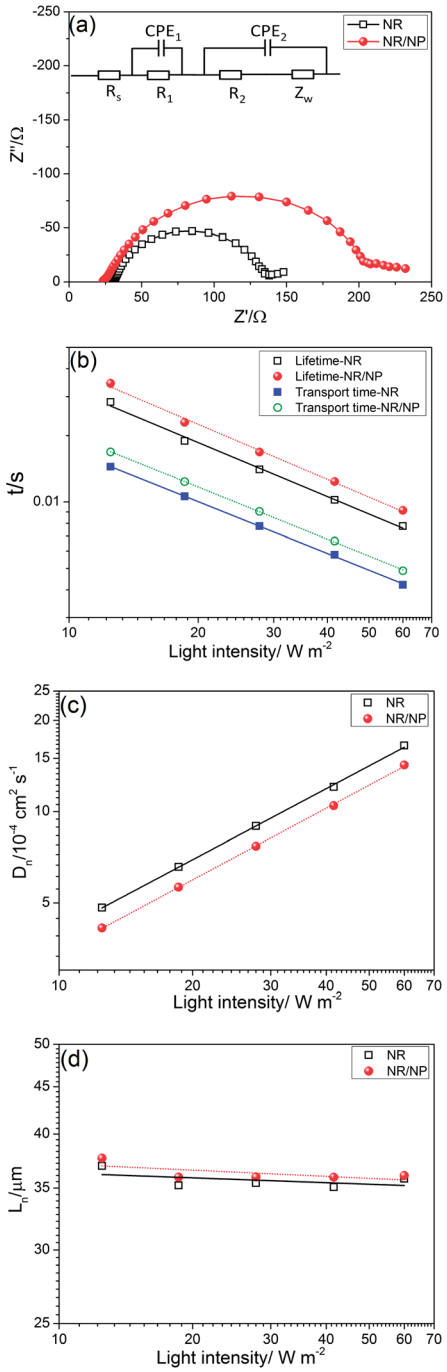

Fig. 6 (a) Nyquist plots under dark conditions with −0.8 V bias voltage (b) electron collection time and lifetime obtained from IMPS and IMVS characterization respectively (c) electron diffusion coefficient D_n and (d) the electron diffusion length L_n as a function of light intensity for DSSCs based on ZnO NR and NR/NP photoanodes.

Table 2 The resistance fitted from the electrochemical impedance spectra of DSSCs based on ZnO NR and NR/NP photoanodes

Samples	R_s/Ω	R_1/Ω	R_2/Ω
NRs	28.4	5.6	105
NRs/NPs	23.2	6.3	178

Fig. 6(b) shows the time constants of electron transport (τ_c) and electron lifetime (τ_r) as a function of light intensity, showing that all time constants decrease with increasing light intensity. The ZnO NR/NP anode showed a longer electron lifetime than NRs, which is due to its weaker charge recombination than the NR anode. On the other hand, the transport time (obtained from IMPS measurement) of a ZnO NR/NP based cell is longer than that of a NR based cell which could be attributed to the presence of numerous boundaries between the ZnO nanorod and nanoparticle branches according to the HRTEM results shown in Fig. 3. As the electron transport time of the ZnO NR/NP structure is larger, its electron diffusion coefficient (D_n) is smaller than that of ZnO NRs which is calculated by the equation $D_n = L^2/2.35\tau_c$, and is shown in Fig. 6(c).[34] The results of IMVS and IMPS also could be explained by a dominant surface diffusion hypothesis.[35]

The electron diffusion length ($L_n = (D_n\tau_r)^{0.5}$) suggests whether the injected electrons can be transported to the external circuit which influences the J_{sc} and PCE.[36] Fig. 6(d) represents the L_n of DSSCs based on ZnO NR and NR/NP structures, which is the same for both *i.e.* about 36 μm, almost without any differences, indicating that L_n had been maintained while changing from the NR structure to the NR/NP structure. This result is better than that reported before. As a result, we fabricated our film with such a thickness (about 38 μm) to maximize the conversion efficiency of DSSCs (see Fig. S2†). The maintained L_n also enables the NR/NP structure to increase the photocurrent and FF and maintain the V_{oc}, thus enhancing the conversion efficiency significantly.

4. Conclusions

A novel ZnO NR/NP hierarchically structured film on a zinc foil has been fabricated through a facile chemical bath deposition method at low temperature. Such ZnO NR/NP hierarchically structured films demonstrated enhanced dye-loading and electron life time when used as photoanodes as compared to ZnO NRs. It also retarded the charge recombination and maintained the electron diffusion length of NRs. As a result, it increased the conversion efficiency of the DSSCs with a significant 169% relative enhancement compared to that based on ZnO NRs.

Acknowledgements

This work has been supported in part by the US Department of Energy, Office of Basic Energy Sciences, Division of Materials and Engineering under Award no. DE-FG02-07ER46467 (Q.F.Z.) on the microstructure characterization and some power conversion efficiency measurements, the National Science Foundation (DMR-1035196), the National Natural Science Foundation of China under Grant no. 51273104 and the National Key Basic Research and Development Program of China under Grant no. 2009CB930602.

Notes and references

1 B. Oregan and M. Gratzel, *Nature*, 1991, **353**, 737–740.
2 A. Yella, H. W. Lee, H. N. Tsao, C. Y. Yi, A. K. Chandiran, M. K. Nazeeruddin, E. W. G. Diau, C. Y. Yeh, S. M. Zakeeruddin and M. Gratzel, *Science*, 2011, **334**, 629–634.
3 A. Hagfeldt, G. Boschloo, L. Sun, L. Kloo and H. Pettersson, *Chem. Rev.*, 2010, **110**, 6595–6663.
4 Q. Zhang, C. S. Dandeneau, X. Zhou and G. Cao, *Adv. Mater.*, 2009, **21**, 4087–4108.
5 Q. Zhang, T. R. Chou, B. Russo, S. A. Jenekhe and G. Cao, *Angew. Chem., Int. Ed.*, 2008, **47**, 2402–2406.
6 N. Memarian, I. Concina, A. Braga, S. M. Rozati, A. Vomiero and G. Sberveglieri, *Angew. Chem., Int. Ed.*, 2011, **50**, 12321–12325.
7 Y. Shi, C. Zhu, L. Wang, C. Zhao, W. Li, K. K. Fung, T. Ma, A. Hagfeldt and N. Wang, *Chem. Mater.*, 2013, **25**, 1000–1012.
8 Y. Shi, C. Zhu, L. Wang, W. Li, C. Cheng, K. M. Ho, K. K. Fung and N. Wang, *J. Mater. Chem.*, 2012, **22**, 13097–13103.
9 C. Cheng, Y. Shi, C. Zhu, W. Li, L. Wang, K. K. Fung and N. Wang, *Phys. Chem. Chem. Phys.*, 2011, **13**, 10631–10634.
10 Y. Shi, K. Wang, Y. Du, H. Zhang, J. Gu, C. Zhu, L. Wang, W. Guo, A. Hagfeldt, N. Wang and T. Ma, *Adv. Mater.*, 2013, **25**, 4413–4419.
11 S. Ito, N.-L. C. Ha, G. Rothenberger, P. Liska, P. Comte, S. M. Zakeeruddin, P. Pechy, M. K. Nazeeruddin and M. Graetzel, *Chem. Commun.*, 2006, 4004–4006.
12 X. Liu, Y. Luo, H. Li, Y. Fan, Z. Yu, Y. Lin, L. Chen and Q. Meng, *Chem. Commun.*, 2007, 2847–2849.
13 Y.-H. Lai, C.-Y. Lin, H.-W. Chen, J.-G. Chen, C.-W. Kung, R. Vittal and K.-C. Ho, *J. Mater. Chem.*, 2010, **20**, 9379–9385.
14 L.-Y. Lin, M.-H. Yeh, C.-P. Lee, C.-Y. Chou, R. Vittal and K.-C. Ho, *Electrochim. Acta*, 2012, **62**, 341–347.
15 T. Guo, Y. Chen, L. Liu, Y. Cheng, X. Zhang, Q. Li, M. Wei and B. Ma, *J. Power Sources*, 2012, **201**, 408–412.
16 J.-Y. Liao, B.-X. Lei, H.-Y. Chen, D.-B. Kuang and C.-Y. Su, *Energy Environ. Sci.*, 2012, **5**, 5750–5757.
17 M. Ye, X. Xin, C. Lin and Z. Lin, *Nano Lett.*, 2011, **11**, 3214–3220.
18 C. Xu, J. Wu, U. V. Desai and D. Gao, *J. Am. Chem. Soc.*, 2011, **133**, 8122–8125.
19 C. Y. Jiang, X. W. Sun, K. W. Tan, G. Q. Lo, A. K. K. Kyaw and D. L. Kwong, *Appl. Phys. Lett.*, 2008, **92**, 143101–143103.
20 W. Chen, Y. Qiu and S. Yang, *Phys. Chem. Chem. Phys.*, 2010, **12**, 9494–9501.
21 W. Chen, Y. Qiu and S. Yang, *Phys. Chem. Chem. Phys.*, 2012, **14**, 10872–10881.
22 Q. Zhang and G. Cao, *J. Mater. Chem.*, 2011, **21**, 6769.
23 S. Yodyingyong, Q. Zhang, K. Park, C. S. Dandeneau, X. Zhou, D. Triampo and G. Cao, *Appl. Phys. Lett.*, 2010, **96**, 073115.
24 L.-Y. Chen and Y.-T. Yin, *Nanoscale*, 2013, **5**, 1777–1780.
25 J. Tian, Q. Zhang, L. Zhang, R. Gao, L. Shen, S. Zhang, X. Qu and G. Cao, *Nanoscale*, 2013, **5**, 936–943.
26 H. Dong, L. Wang, R. Gao, B. Ma and Y. Qiu, *J. Mater. Chem.*, 2011, **21**, 19389–19394.
27 Y. Shi, C. Zhan, L. Wang, B. Ma, R. Gao, Y. Zhu and Y. Qiu, *Adv. Funct. Mater.*, 2010, **20**, 437–444.
28 R. Gao, Z. Liang, J. Tian, Q. Zhang, L. Wang and G. Cao, *RSC. Adv.*, 2013, **3**, 18537–18543.
29 R. Gao, Z. Liang, J. Tian, Q. Zhang, L. Wang and G. Cao, *Nano Energy*, 2013, **2**, 40–48.
30 R. Gao, L. Wang, Q. Zhang and G. Cao, *ECS Trans.*, 2013, **45**, 127–135.
31 X. F. Wu, H. Bai, C. Li, G. W. Lu and G. Q. Shi, *Chem. Commun.*, 2006, 1655–1657.
32 R. Gao, J. Tian, Z. Liang, Q. Zhang, L. Wang and G. Cao, *Nanoscale*, 2013, **5**, 1894–1901.
33 J. B. Baxter and E. S. Aydil, *Sol. Energy Mater. Sol. Cells*, 2006, **90**, 607–622.
34 S. Nakade, Y. Saito, W. Kubo, T. Kitamura, Y. Wada and S. Yanagida, *J. Phys. Chem. B*, 2003, **107**, 8607–8611.
35 M. J. Yang, B. Ding, S. Lee and J. K. Lee, *J. Phys. Chem. C*, 2011, **115**, 14534–14541.
36 W.-Q. Wu, H.-S. Rao, Y.-F. Xu, Y.-F. Wang, C.-Y. Su and D.-B. Kuang, *Sci. Rep.*, 2013, **3**, 1892.